Copyright WILEY-VCH Verlag GmbH & Co. KGaA, 69469 Weinheim, Germany, 2020.

Supporting Information

for *Small Methods,* DOI: 10.1002/smtd.202000072

Wafer-Scale Fabrication of Nanopore Devices for Single-Molecule DNA Biosensing using MoS_2

*Mukeshchand Thakur, Michal Macha, Andrey Chernev, Michael Graf, Martina Lihter, Jochem Deen, Mukesh Tripathi, Andras Kis, and Aleksandra Radenovic**

SUPPLEMENTARY INFORMATION for

Wafer-scale Fabrication of Nanopore Devices for Single-Molecule DNA Biosensing using MoS_2

Mukeshchand Thakur,[1⊥] Michal Macha,[1⊥] Andrey Chernev,[1] Michael Graf,[1] Martina Lihter,[1] Jochem Deen,[1] Mukesh Tripathi,[2] Andras Kis[2] and Aleksandra Radenovic[1]*

[1]Institute of Bioengineering, Laboratory of Nanoscale Biology, [2]Laboratory of Nanoscale Electronics and Structure, Institute of Electrical Engineering and Institute of Materials Science and Engineering, School of Engineering, EPFL, 1015 Lausanne, Switzerland

⊥ These authors contributed equally

*All correspondences should be addressed to aleksandra.radenovic@epfl.ch

---

Table of Contents

Figure S1. Schematic of the homemade MOCVD setup and MoS_2 synthesis.

Figure S2. Optical images of a MoS_2 film under different growth conditions.

Figure S3. Microfabrication steps involved in wafer-scale substrate fabrication.

Figure S4. Substrate aperture variability and quality characterization.

Figure S5. Optical images of a MoS_2 monolayer film grown over a large area.

Figure S6. Photoluminescence measurements.

Figure S7. STEM imaging and large-field of view (FOV) of continuous MoS_2 after transfer.

Table S1. Comparison of wafer-scale transfer efficiency of MoS_2 using PDMS among different batches of substrates.

Figure S8. Optical images showing examples of unsuccessful transfer of MoS_2 on SiN_x membrane.

Figure S9. TEM images showing comparison cleanliness of PDMS and PMMA polymers post-transfer of MoS_2.

Figure S10. *I-V* measurement for Device A.

Figure S11. DNA translocation measurements and analysis from Device B.

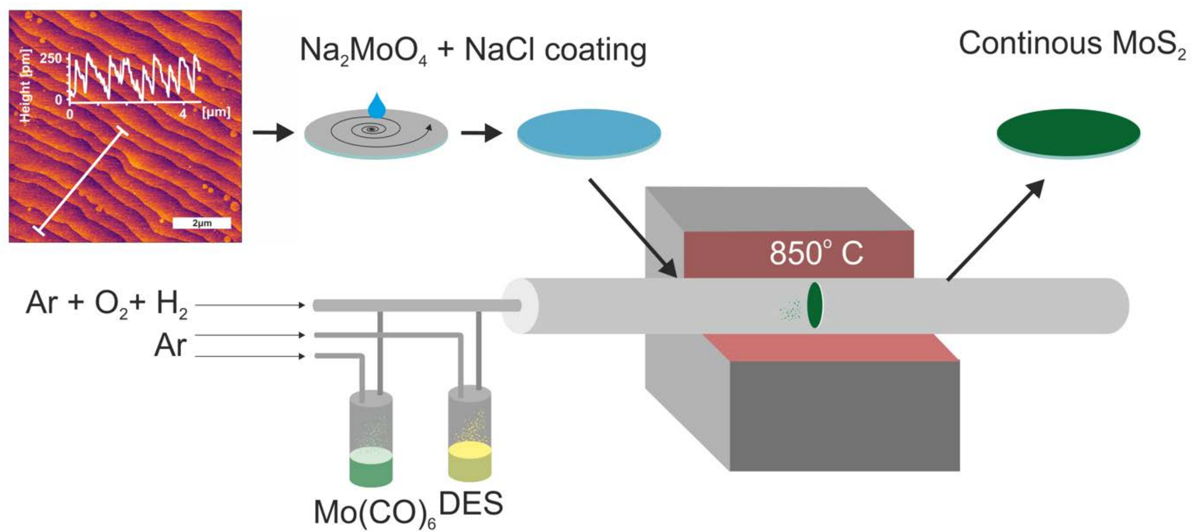

Figure S1. Schematic of the custom-made MOCVD setup for the MoS_2 monolayer synthesis. The annealed c-plane sapphire 3-inch wafer is spin-coated with growth promoter (mixture of Na_2MoO_4 and NaCl) and placed in a tube furnace. Growth step is performed in ambient pressure and at 850° C.

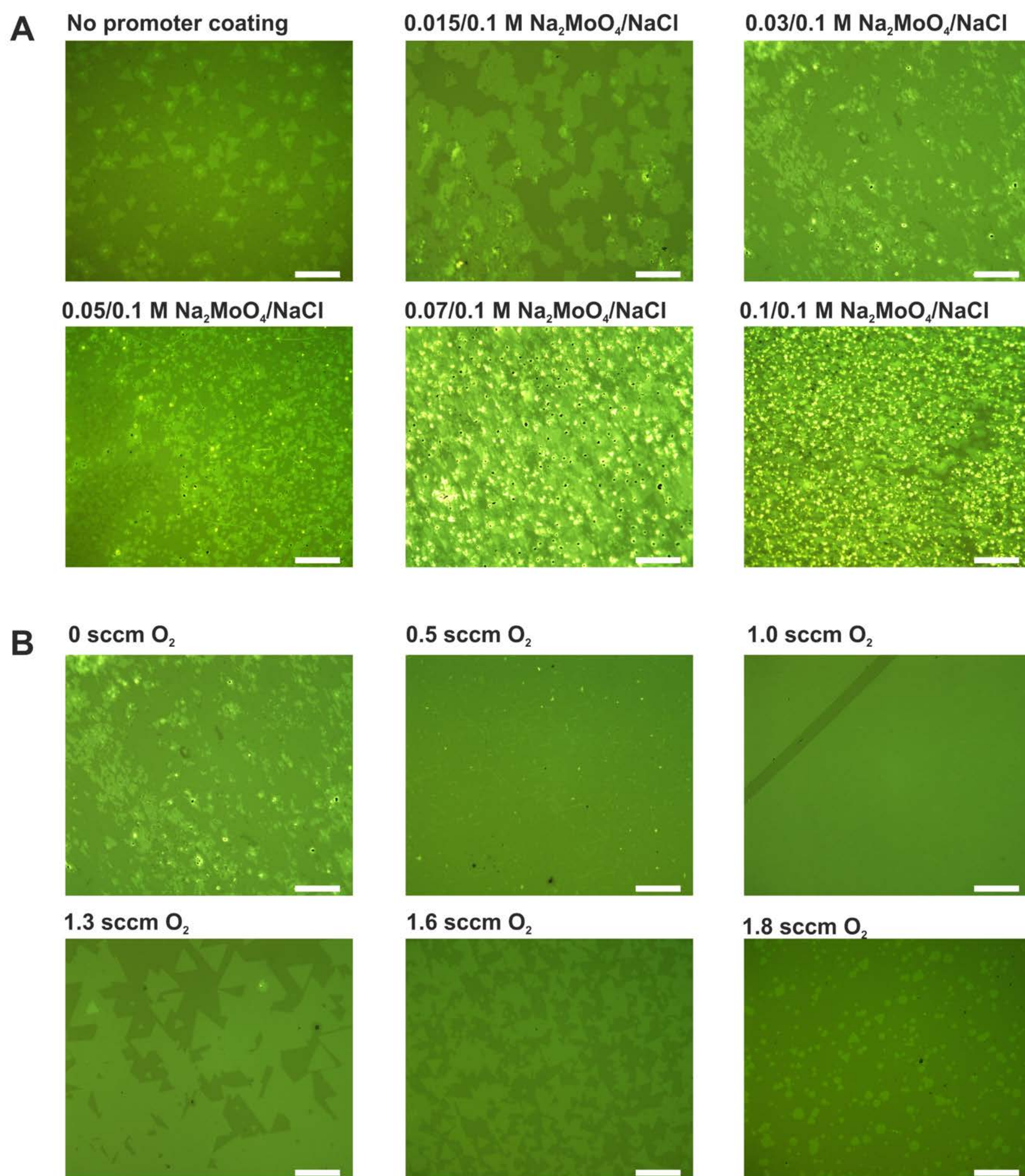

Figure S2. Optical images of a MoS_2 grown under different process conditions showing (a) an impact of precursor solution concentration ratio over a growth thickness. The growth process was done at 210 sccm of Ar, 3 sccm of diethyl sulphide, 12 sccm of $Mo(CO)_6$, 4 sccm of H_2 and 0 sccm off O_2 at 850° C for 30min. (b) a growth results influenced by the addition of slight O_2 flow to the reaction. The growth conditions were the same as in (a) with a constant precursor concentration of 0.03 M / 0.1 M and varying oxygen flow. All scale bars are 50 μm.

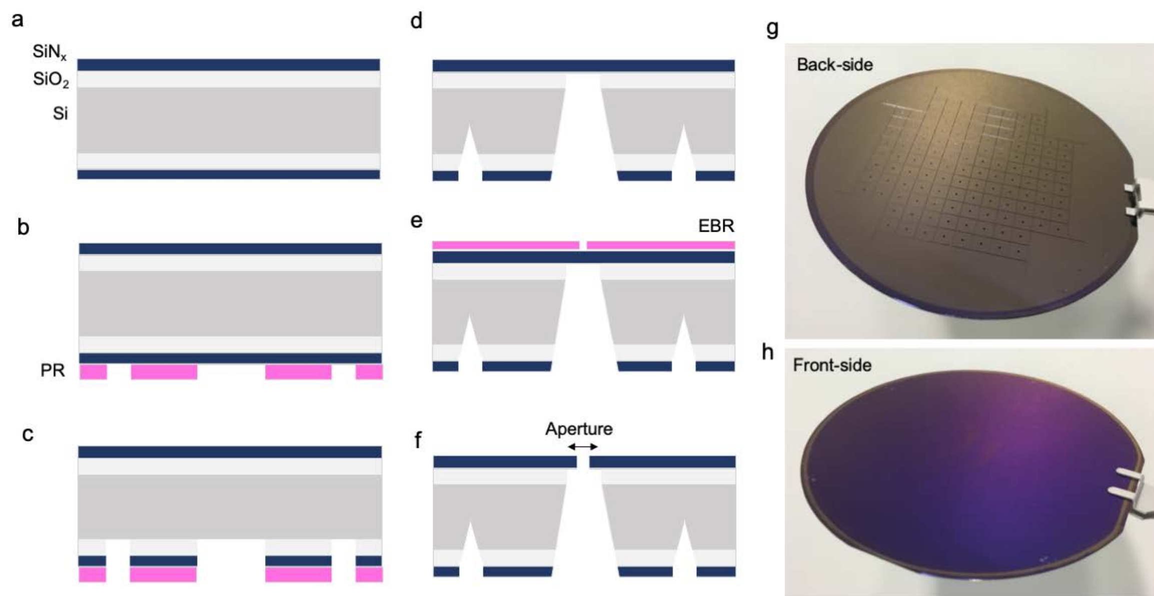

Figure S3. Substrate fabrication. Wafer-scale process of the supporting SiN_x chips preparation is explained step by step: double side polished 380 μm thick Si (100) 100 mm diameter wafer (darker grey) with 60 nm of SiO_2 (lighter grey) and 20 nm of SiN_x (dark blue) on each side (a) is being processed with back-side photolithography, pink for photoresist (PR) layer (b) and the pattern is transferred using dry etching (c). The aperture is exposed to 25% wt KOH to form the SiN_x membranes and dicing lines (d). The ~80 nm apertures in the middle of each membrane are being formed using e-beam lithography, pink for e-beam resist (EBR) layer (e) and a consequent dry etching (f). The resulting wafer design is shown from the back side (g) and the front side (h).

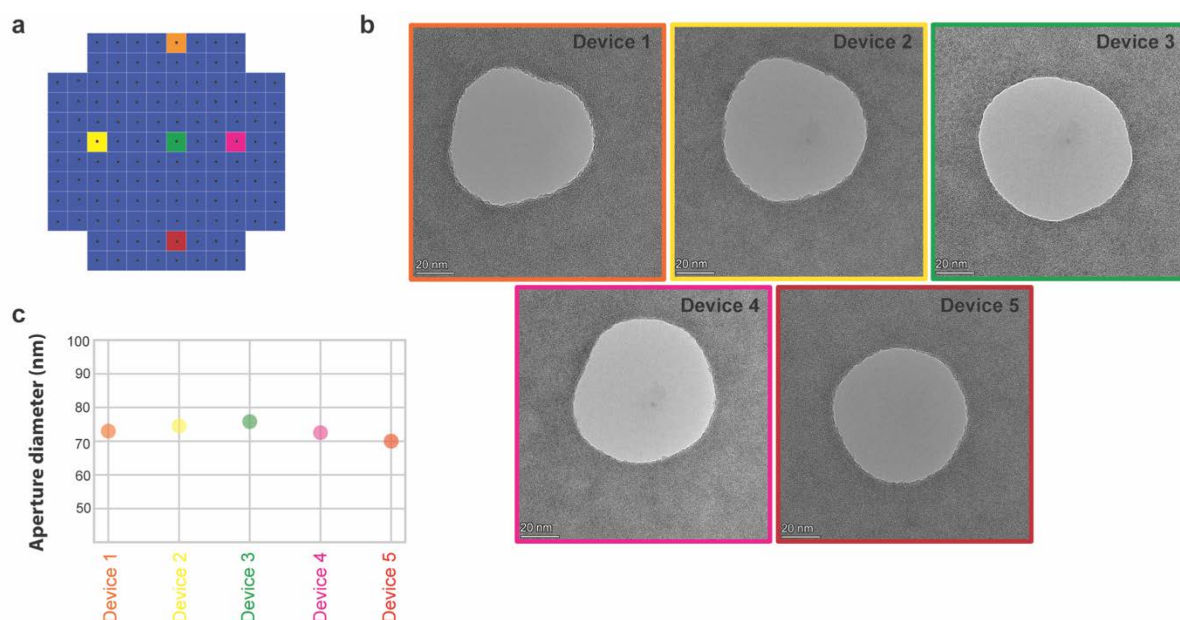

Figure S4. Substrate aperture variability and quality characterization. (a) Representative sites on the wafer from where five devices are used to characterize their aperture size and cleanliness before transfer. Presence of bulky residues around the aperture causes blister formation after the transfer of MoS_2. (b) TEM images of respective devices show the aperture openings and showed clean surface. (c) The aperture diameter was ~75 nm showing similar sizes and very low substrate variation (<5% error), estimated using Image J.

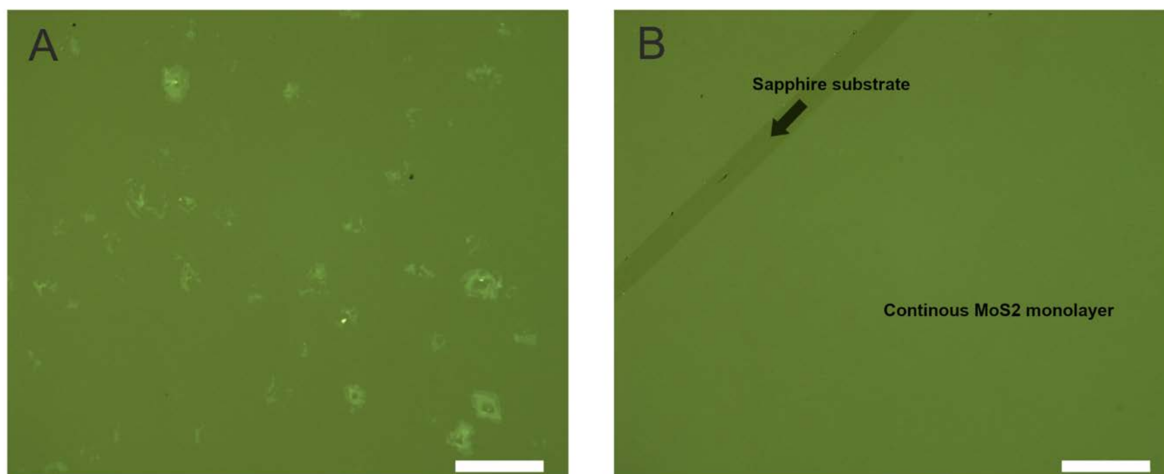

Figure S5. Optical images of a MoS_2 monolayer film grown over a large area from the same batch. (a) with visible extruded grain boundaries and secondary nucleation sites where the spin-coated solution was the thickest (around the edges of the substrate) representing roughly ~10% of the substrate area, and (b) with a clean, continuous monolayer surface visible on the remaining area. Scale bars are 50 μm.

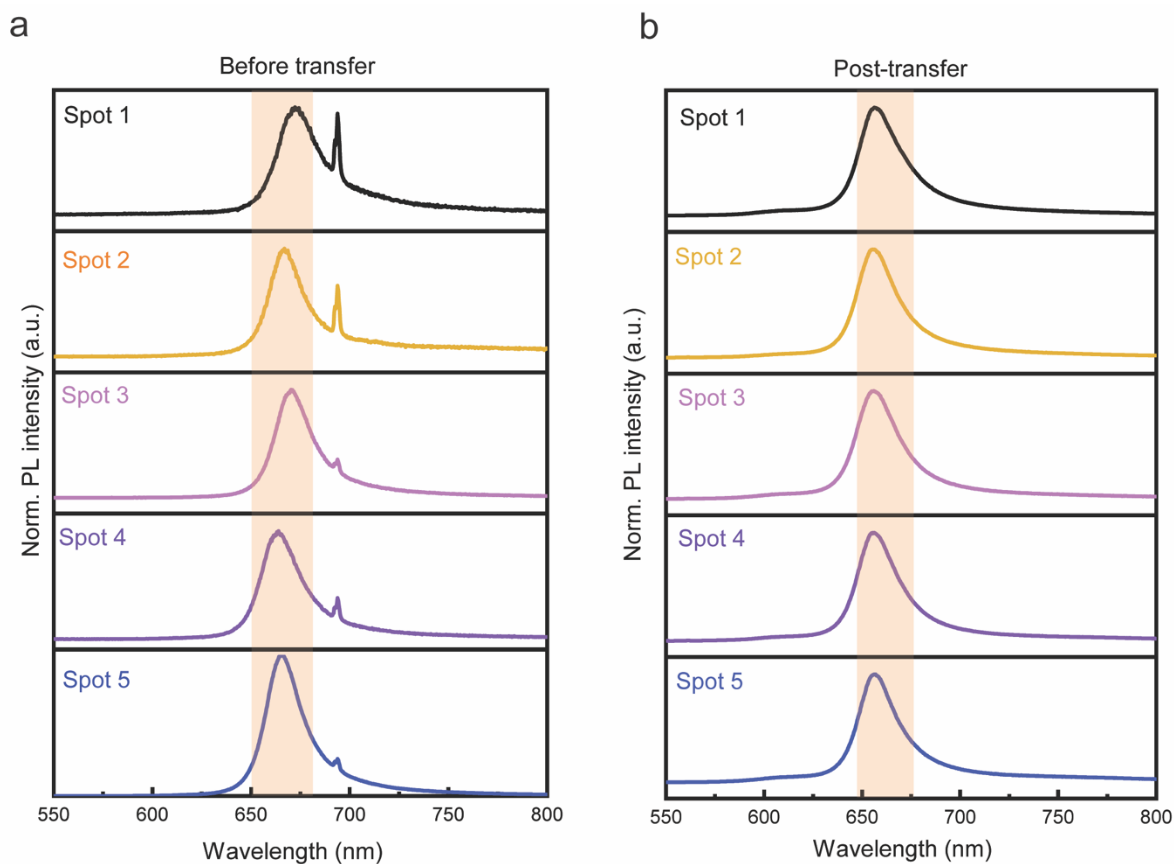

Figure S6. Photoluminescence measurements. (a) As-grown MoS_2 on the sapphire substrate from five different spots (shown in Figure 2a-b in the manuscript) before and (b) after the transfer on SiN_x surface. The shaded region in the graphs is a guide to the eye showing the peaks corresponding to the MoS_2.

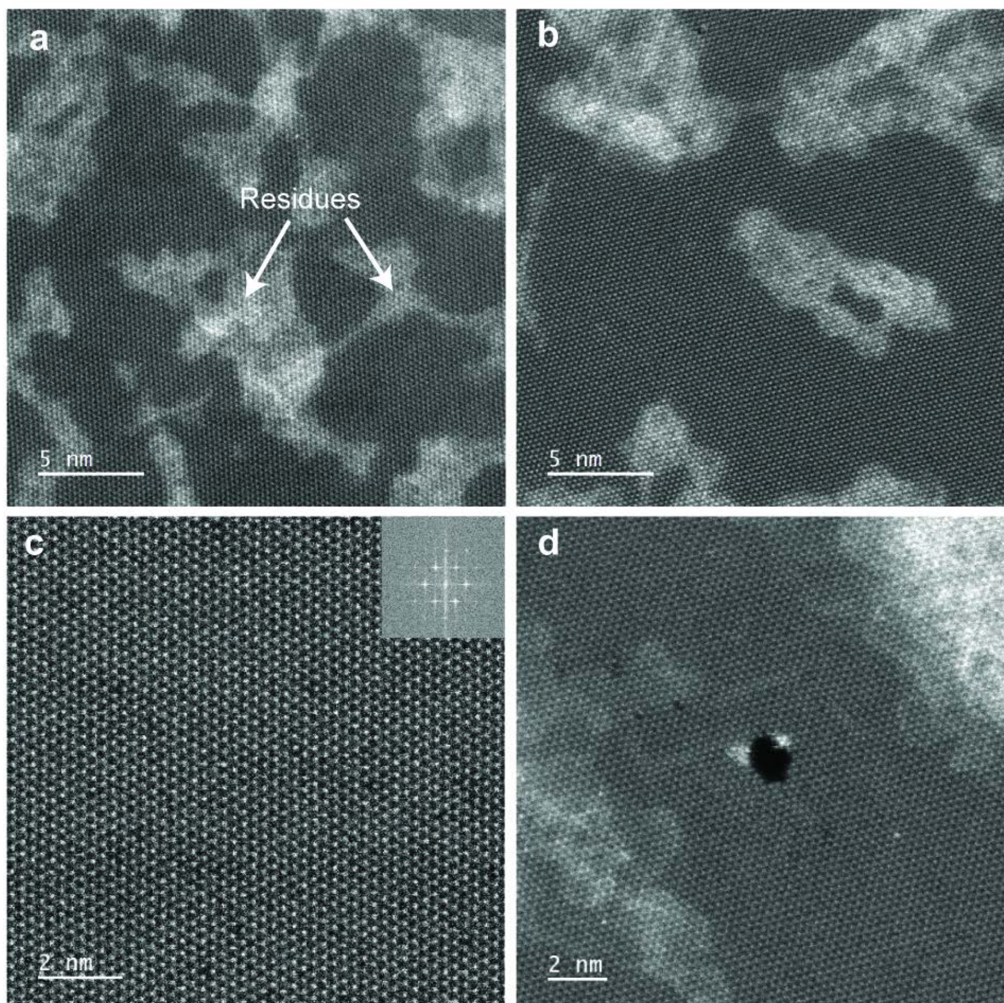

Figure S7. Raw STEM/HAADF images show a large-field of view (FOV) of continuous MoS_2 lattice transferred by PDMS. (a, b) Representative MoS_2 areas with residues (brighter contrast on the panels). (c) High magnification STEM image shows the perfect lattice structure of monolayer MoS_2. The inset image shows the Fast Fourier transform, which further confirms the monolayer structure. (d) A nanopore (~2 nm^2) in the center of the image, formed by the electron-beam probe in STEM.

Table S1. Comparison of wafer-scale transfer efficiency of MoS_2 using PDMS among different batches of substrates. From these wafer-scale transfer, the average transfer efficiency is 70.13±2.4 %.

Batch	*Total chips*	*Successful transfer*	*Unsuccessful transfer*	*Broken SiN_x membrane post-transfer*	*Transfer efficiency (%)*
Batch A	120	83	36	1	69.1
Batch B	128	87	41	0	67.9
Batch C (shown in Figure 3)	128	94	34	0	73.4

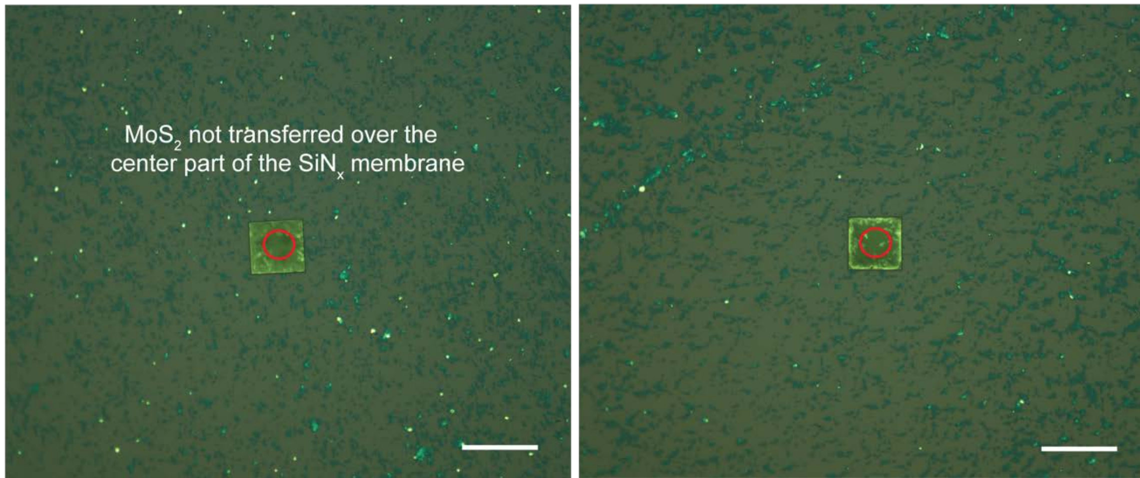

Figure S8. Optical images showing examples of unsuccessful transfer of MoS_2 over the highlighted region where the aperture is located. All scale bars are 50 μm.

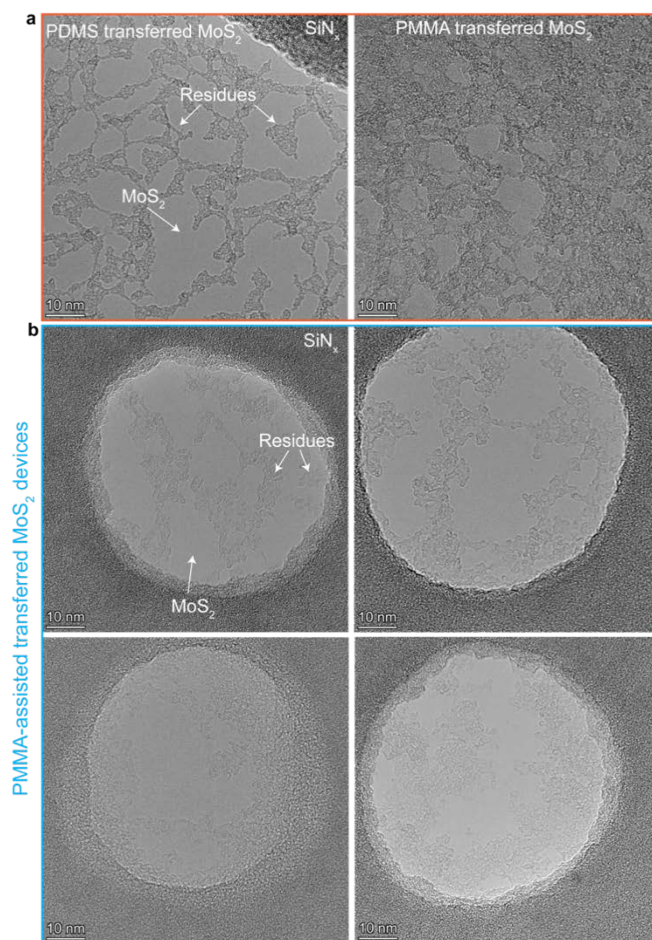

Figure S9. Comparison and cleanliness variation among samples of MoS_2 imaged using TEM. (a) TEM images showing suspended MoS_2 post-transfer using PDMS and PMMA polymers on SiN_x TEM grids. The calculated clean area MoS_2 (without residues) with traditional PMMA was ~20% while with PDMS (current method) was ~50% clean area on the respective MoS_2 samples. The clean regions were calculated using Image J[1]. (b) Representative devices with MoS_2 transferred using traditional PMMA polymer showing variation in cleanliness. These devices show comparable cleanliness with MoS_2 devices transferred using PDMS polymer (Figure 3b in main text).

1.Rueden, C. T. *et al.* ImageJ2: ImageJ for the next generation of scientific image data. *BMC Bioinformatics* **18**, 529 (2017).

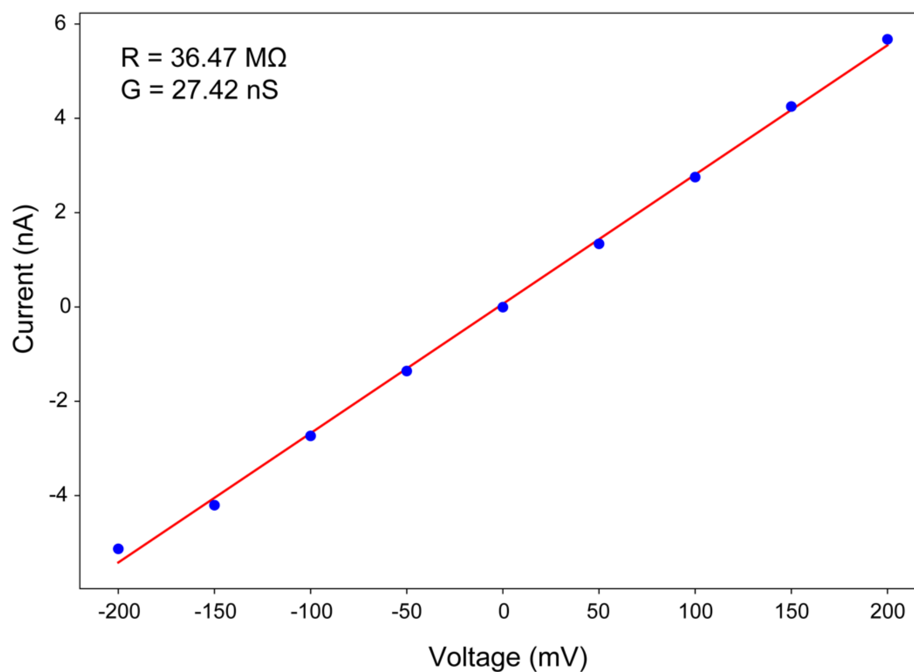

Figure S10. I-V characteristics (Device A). The location of Device A is highlighted in Figure 3a in the manuscript. The I-V response for the MoS_2 nanopore was measured in 1M KCl by sweeping the voltage in the range between -200 mV and +200 mV.

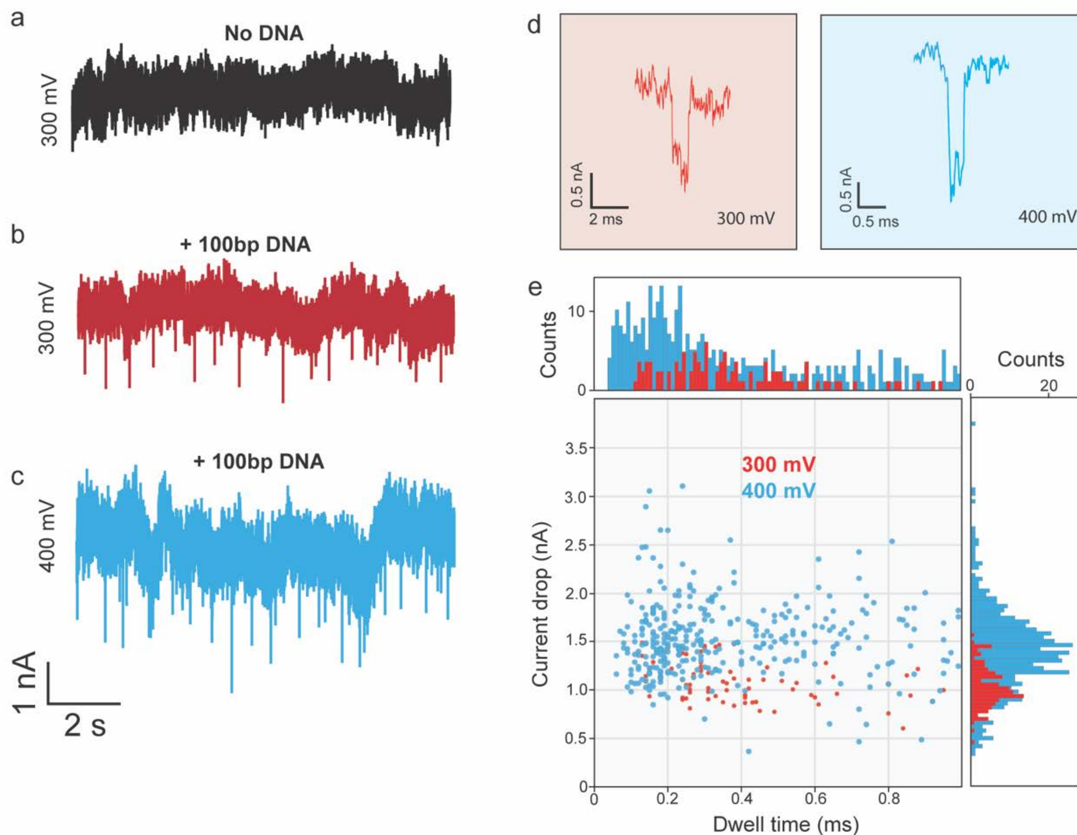

Figure S11. DNA translocation using ~4 nm MoS_2 nanopore (Device B, from a batch number 2 of the wafer transfer) in 1M KCl. (a) Negative control: open-pore current trace at 1M KCl prior addition of DNA. The current trace showed no translocation spikes measured at 300 mV. Current trace (10s) after the addition of 100 bp DNA (10 nM) showing translocation spikes measured at (b) 300 mV and (c) 400 mV. (d) Representative events from the traces obtained in (b and c). (e) Scatter and histogram plots, respectively, of 100 bp DNA translocation events. The events were recorded at 300 mV and 400 mV, and show ~20% current blockades.